Hot strength, dynamic recovery and dynamic recrystallization of 317 type stainless steel

E. EVANGELISTA, Dipartimento di Scienze dei Materiali e della Terra, Università di Ancona, Ancona, Italy
H.J. McQUEEN and N.D. RYAN, Department of Mechanical Engineering, Concordia University, Montreal, Canada

Abstract
Hot torsion tests were performed to fracture on type 317 stainless steel in both the as-cast and the worked condition, at temperatures between 900 and 1200°C and strain rates of 0.1-5 s^{-1} in order to study the microstructure responsible for hot workability behaviour. Each flow curve exhibited a peak followed by a decrease to a steady-state regime as a result of dynamic recovery and dynamic recrystallization. The hypothetical saturation stress due to dynamic recovery and the critical stress for dynamic recrystallization were determined from the strain hardening rate vs stress plots. The dependence of flow stress on temperature followed an Arrhenius function with an activation energy of 508 kJ/mol for the as-cast and 496 kJ/mol for the worked material. The role of δ ferrite particles on dynamic restoration and on mechanical behaviour was analyzed. The subgrain and recrystallized grain sizes were related to the conditions of deformation.

Riassunto
Resistenza a caldo, ripristino e ricristallizzazione dinamici dell'acciaio inossidabile 317
Con lo scopo di studiare il comportamento alla deformazione in funzione della microstruttura sono stati sottoposti a prove di torsione rapida provini dell'acciaio inossidabile 317 a temperature comprese tra 900 e 1200°C con velocità di deformazione di 0.1-5 s^{-1}. Le curve sollecitazione-deformazione mostrano un picco ed una diminuzione verso lo stato stazionario a causa dei fenomeni dinamici di ripristino e di ricristallizzazione. Dalle curve della velocità di incrudimento in funzione della sollecitazione è stato ricavato il valore limite di saturazione della sollecitazione. La dipendenza della sollecitazione dalla temperatura segue una funzione di Arrhenius con energie di attivazione di 508 e 496 kJ/mol per l'acciaio in forma « cast » e « worked » rispettivamente. È stato inoltre studiato il ruolo delle particelle di ferrite δ sui fenomeni dinamici e sul comportamento meccanico, della grandezza dei grani e dei sottograni in funzione delle condizioni di deformazione.

Introduction

Since austenitic stainless steels are subjected to a variety of industrial deformation processes, it is imperative that the mill metallurgists have a knowledge of the deformation characteristics of the alloy, as well as its microstructural behaviour (1,2). Such information could be used to optimize the production of a higher quality material at lower cost. During the hot deformation of austenitic stainless steel, work hardening is reduced by the primary restoration mechanism, dynamic recovery (DRV), until a critical strain at which it is further decreased by the initiation of dynamic recrystallization (DRX). With the predominance of softening over hardening, the flow stress reaches a peak and declines slowly to a steady-state regime. There both restoration mechanisms balance the hardening and counteract grain boundary cracking to give rise to high ductility (3,4).
Since the alloy additions which lead to its prevalent use in the chemical industry also diminish its workability, the deformation of type 317 has been investigated with respect to the effects of temperature, strain and strain rate, which are the prime factors of industrial significance, (5-9). Furthermore, the interrelationship of dislocation density, precipitates and solutes, which have a definite bearing upon the strength and ductility of the alloy have been examined.

Experimental techniques

The type 317 stainless steel, provided by Atlas Steels of Tracy, Quebec, had the same composition for both the as-cast (C) and the worked (W) materials: (wt%) 18.60 Cr, 13.88 Ni, 3.22 Mo, 1.73 Mn, 0.44 Si, 0.035 C, 0.017 N, balance Fe. Torsion specimens, with their axes parallel to the rolling direction, were machined to close tolerances in the gauge section (l = 25.4 mm; 2r = 6.25 mm) to ensure uniform twisting. Annealing for 30 minutes at 1050°C was followed by quenching in water in order to avoid the damaging effects of carbide precipitation. Grain sizes of 57 μm and 72 μm for as-cast and worked specimens respectively were determined by optical microscopy, using the three circle intercept method. In the as-cast material this is the spacing of the dendrites which were separated by 23% δ ferrite. After homogenization for five minutes at the deformation temperature, the specimens were subjected to twisting on a closed-loop, servo-controlled hydraulic torsion machine (10) in the range 900-1200°C at surface strain rates of 0.1 to 5.0 s^{-1}. For calculating the nominal shear stress (τ) from the torque (Γ), the following relationship was used:

$$\tau = (\Gamma/2\,\pi\, r^3)(3 + n' + m) = \bar{\sigma}/\sqrt{3} \qquad (1)$$

whereas the surface shear strain rate ($\dot{\gamma}$) was evaluated from the twists per second as follows:

$$\dot{\gamma} = (\text{revolutions/s})\ (2\,\pi\, r/l) = \sqrt{3}\,\dot{\bar{\varepsilon}} \qquad (2)$$

While the value of the strain hardening coefficient (n') was taken as zero (11) at the peak stress (σ_p), the value of the strain rate sensitivity (m) was evaluated across the entire testing range. The subsequent equivalent flow stress (σ) and strain (ε) were calculated using the von Mises criterion. In this paper, the values of σ and ε are intended as equivalent and are written without bars over them.
After testing, the specimens were quenched to preserve the hot worked microstructure. Tangential, longitudinal and transverse sections were examined by

optical metallography and grain sizes determined as above.
Slices for TEM examinations were cut, at 0.5 mm below the surface, longitudinally parallel to the axis of torsion, by means of a slowly running diamond cut-off saw, in order to avoid disturbance of the developed microstructure. After being ground parallel, they were chemically thinned to 50 μm with a solution of 20% perchloric acid in butoxyethanol at -4°C and 18 V. Finally, 3 mm discs, punched from the slices, were prepared by double-jet thinning with the same solution and operating conditions. The TEM microstructural analysis was performed on a Philips CM 12 electron microscope at 120 KV. The subgrain sizes were determined by the linear intercept method, the mean intercept being multiplied by 1.68 to determine the mean subgrain diameter (12).

Results

The representative stress-strain curves in Fig. 1 illustrate the comparative behaviour of as-cast and worked 317 steel. While the materials, in both conditions, strain harden at low strains rising to a peak stress, σ_p, and peak strain, ε_p, the as-cast material fractured shortly after at $\varepsilon_f = 1$ to 2. The worked metal underwent flow softening to a steady state regime, where fracture occurred at strains of the order of 10. During straining, both materials are subject to the restorative softening mechanisms of DRV and DRX. In addition, ε_p and σ_p decrease in the usual manner with increasing temperature and decreasing strain rate. The as-cast material has a higher σ_p and lower ε_p because the large δ ferrite particles cause additional hardening and enhance nucleation for DRX (13).
The σ-ε curves, (Fig. 1), were further analyzed by determining the strain hardening rate ($\theta = d\sigma/d\varepsilon$) at a series of points along the flow curve up to σ_p, (Fig. 2), (8,14). The work-hardening rate decreases more steeply as the Zener-Hollomon parameter Z decreases. Primarily consisting of two distinct segments, each curve decreases linearly to a point where its rate of decline is reduced by subgrain formation (15). Thereafter, the flow stress decreases less per unit of strain than in the earlier regime. Then the curve starts

Fig. 1 - Typical equivalent stress-equivalent strain curves for 317 stainless steel. Dotted lines represent the values of saturation stress, derived from Fig. 2 by extrapolating the lower linear segment. Intersecting bars ╲, |, indicate the critical strain for the beginning of dynamic recrystallization ε_c and the strain to the peak ε_p, respectively; ε_f is the fracture strain.

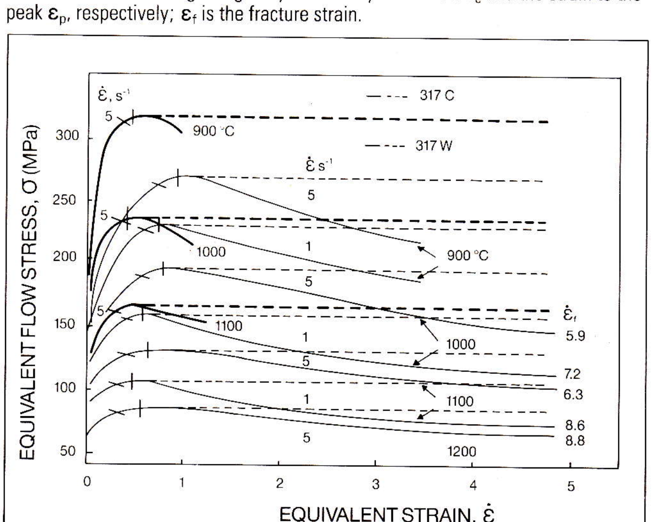

Fig. 2 - Strain hardening rate θ versus flow stress, σ, curves for a) as-cast and b) worked 317 steel, indicating the critical stress σ_c for dynamic recristallization, the peak stress σ_p and the saturation stress σ^*_s (extrapolating to $\theta = 0$).
$\dot{\varepsilon}$ = — 5 s^{-1}, --- 1 s^{-1}, — 0.1 s^{-1}.

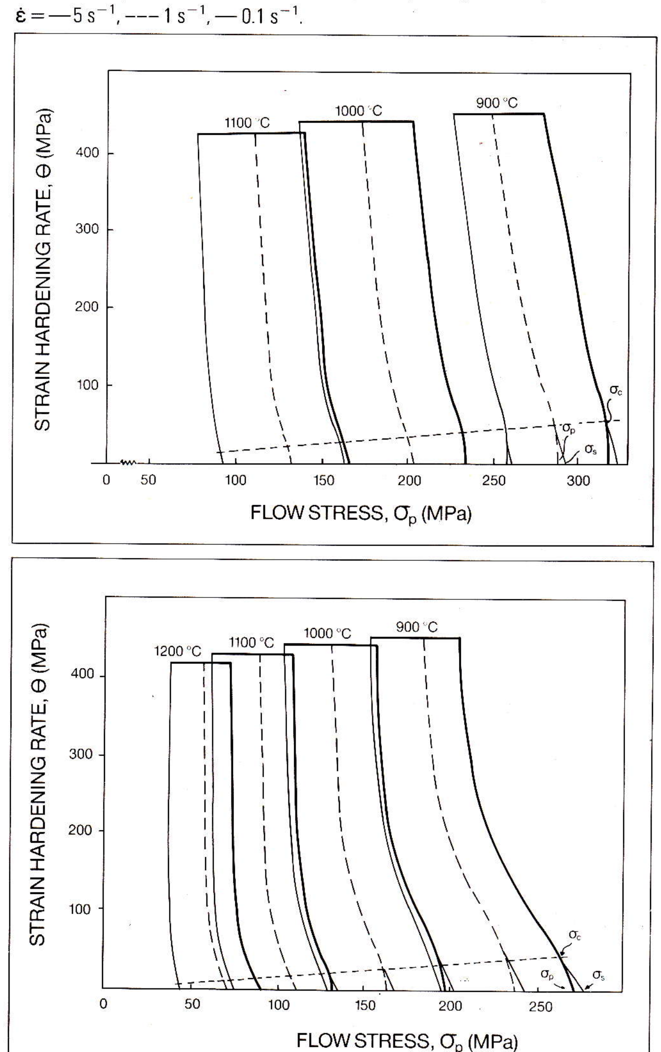

to fall rapidly to zero at the point of DRX initiation. In the absence of this last softening mechanism, the θ - σ curve would continue to decrease linearly to zero, with the establishment of a saturation stress (σ_s*) due to DRV alone. The values are shown in Fig. 1. The upward extrapolations of the θ - σ curves to $\sigma = 0$, for all deformation conditions, converge to a common point which increases with the metallic solute content (8). The values for the as-cast materials are slightly higher. The critical stress for DRX increases (16) linearly as Z increases. The strain hardening of 317C is higher than 317W because of δ ferrite particles causing the formation of fine dislocation cells.
The dependence of the peak stress on temperature and strain rate (Fig. 3) follows a relationship of the form (17):

$$A \sinh (\alpha \sigma_p)^n = \dot{\varepsilon} \exp (Q/RT) = Z \qquad (3)$$

were A, α, n, Q are empirical constants and R is the universal gas constant. The values of n are close to those of creep. The function A' exp (β σ) was also found suitable for the as-cast data, but the function A" σ^n gave n values rising with ε. The apparent activation energies, Q, were derived from the slopes in Fig. 4. For the as-cast and worked materials, they were determined as 508 and 496 kJ/mol respectively.
Fig. 5 shows the behaviour of yield-stress, σ_y, and that of the steady state stress, σ_s, with Z. At high Z values for which σ_y is almost athermal, the strain hardening and σ_s increase rapidly as Z rises. As Z decreases, the narrowing space between the σ_y and σ_s curves shows the continuing effect of DRV and DRX.
Optical micrographs of samples tested to fracture, or to a steady state, show recrystallized equiaxed grains, smaller than the original ones, for all conditions, (Fig. 6).

Fig. 3 - The interdependence of strain rate and peak stress confirms the hyperbolic sine relationship.

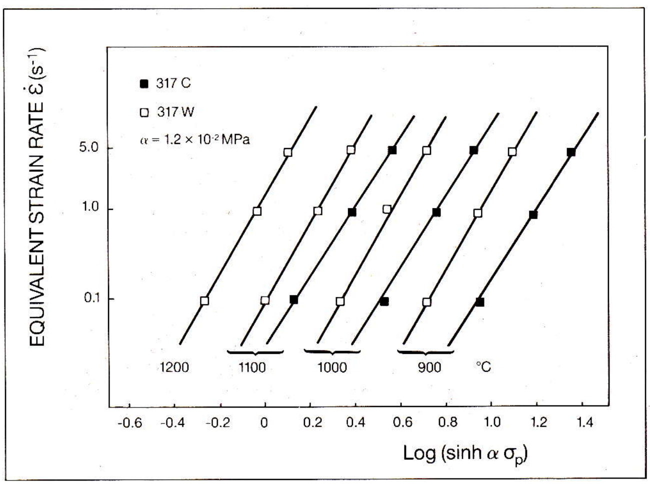

Fig. 4 - The flow stress, strain rate and temperature interdependence follow an Arrhenius relationship. The values of Q were found to be 508 and 496 kJ/mol for as-cast and worked respectively.

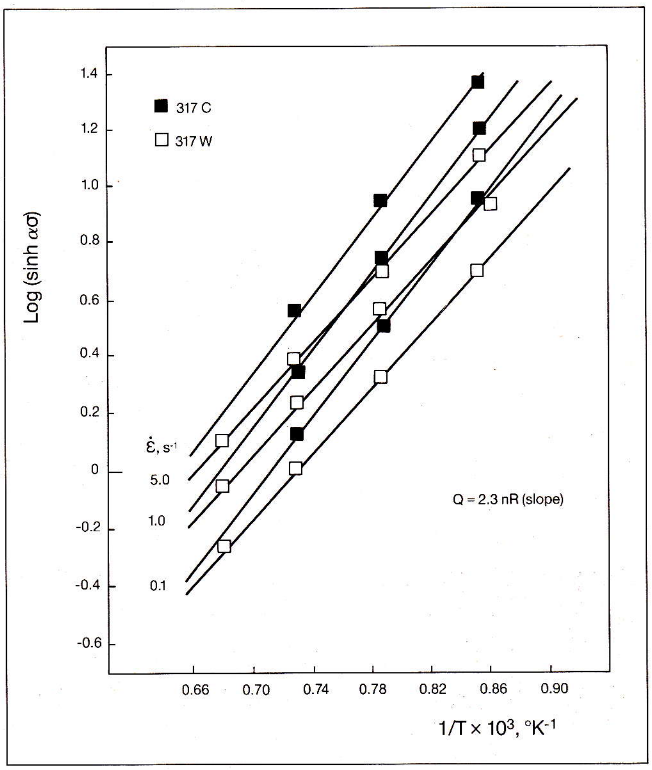

Fig. 5 - Effect of temperature corrected strain rate on σ_y yield and σ_s steady-state stresses. Temperature scales given for $\dot{\varepsilon} = 1.0\ s^{-1}$.

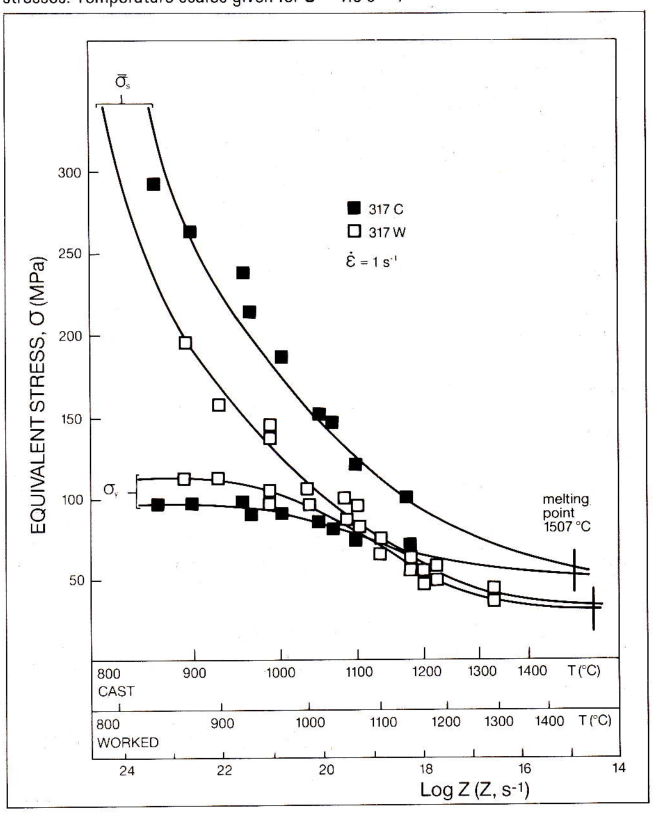

Fig. 6 - Optical micrographs showing the recrystallized grain size with precipitates in the cast.
a) 317C: 1) as-cast; 2) 1000°C, 0.1 s^{-1}; 3) 1000°C, 1 s^{-1}.
b) 317W, $\dot{\varepsilon} = 1.0$ s^{-1}: 1) 900°C; 2) 1000°C; 3) 1200°C.

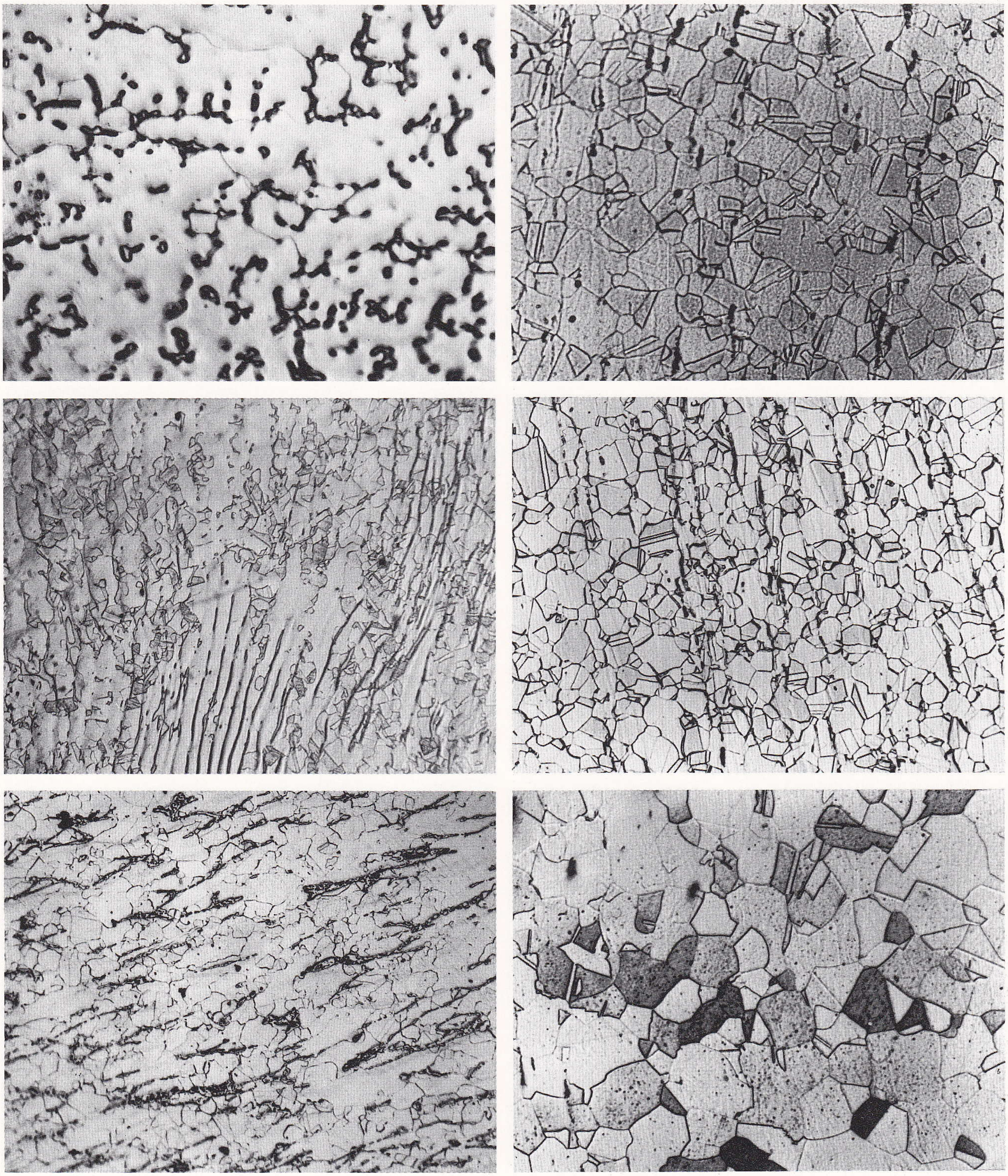

1 1
2 2
3 3

(a) (b)

The plot of recrystallized grain diameters, D_s, vs Z, (Fig. 7), is linear. Combined with the power-law approximation of equation 3, this shows that the data points are well fitted by the relationship:

$$D_s = K\,\sigma^N \qquad (4)$$

were K and N are constants, the latter having values between 0.7 and 0.8 (1,18).
The TEM micrographs show different microstructures for as-cast and worked specimens with respect to Z. For high Z values, both as-cast and worked materials exhibit subgrain structures elongated in the stress direction. For low Z, the as-cast material shows equiaxed subgrains with dislocations inside and sometimes the occurrence of an undissolved δ phase on the boundaries, (Fig. 8). Subgrain diameters, d_s, are plotted versus log Z, (Fig. 9), fitting the equations (8,19-21):

$$d_s = K'\,\sigma_s^{-1} \qquad (5)$$

$$\text{as-cast } d_s^{-1} = -1.82 + 0.15 \log Z \qquad (6)$$

$$\text{worked } d_s^{-1} = -2.55 + 0.15 \log Z \qquad (7)$$

where K' is a material constant.
The ductility of worked 317 steel increases with rising temperature and falling strain rate. In Fig. 10, the ductility of the as-cast and worked materials are compared to each other and to equivalent data for 304. In these austenitic steels, the significant mechanism improving ductility is dynamic recrystallization which impedes the growth of grain boundary cracks as the boundaries migrate away from them (2-4).
The strain to fracture in 317W is lower than in 304W because higher solute and precipitate levels retard the recrystallization. The worked 317 is superior to the as-cast because the δ phase has been reduced and spheroidized. In the 304W, the δ ferrite and other solidification segregates have been largely eliminated (5-7, 21-22). The ductility rises with temperature because the recrystallization is speeded up by increased thermal activation and solution of precipitates. In type 304W, the increase in strain rate over this limited range also raises the recrystallization rate and the ductility by raising the driving force. On the other hand in 317W, the increased alloying slows the impeding effects of DRX sufficiently that it is unable to keep up with enhanced cracking at higher strain rate and stress. However at 1200°C in Fig. 10, the ductility is almost independent of $\dot{\varepsilon}$.

Discussion

The flow curves of 317, like 304 steel, exhibit the classic form of dynamic recrystallization (Fig. 1). The reduction of strain hardening by DRV during initial straining is confirmed by the θ - σ plots (Fig. 2). The change from high to low slope segments in the θ - σ plots of 304W was shown by Carfi et al. (15) to result from the evolution of disordered tangles into sharper, more ordered sub-boundaries. The occurrence of DRX near the peak is confirmed by the presence of equiaxed grains in both as-cast and worked specimens (Fig. 6). In the former, the mechanism is so slowed by the presence of δ ferrite, that it is unable to retard the grain boundary cracking; thus, fracture occurs before the steady state is attained.
The strain hardening rate of the as-cast alloy is much higher than that of the homogenized worked one (Fig. 2) because of the larger volume fraction of δ in the former (23% compared to about 4%). The δ particles disrupt flow in the γ phase causing the formation of fine, highly misoriented cells which raise the strength but also convert into nuclei for DRX (2, 4, 9). Similar relative behaviour has been observed in parallel studies in 304 and 316, in which homogenization and working dissolved all the ferrite (6, 7). Comparison of as-cast or worked behaviour shows that 317 is stronger than 304 or 316 alloys because of both higher δ content and solute level. At lower temperatures the strength is also raised by the interaction of the Mo with C and N. The ε_p in 317C or 317W are less than those of 304 and 316 because of greater δ levels (8,9). The final sudden turn down of the θ - σ curves (Fig. 2) permit precise determination of ε_c for DRX at 0.65 ε_p for 317W and 0.72 ε_p for 317C. This compares with 0.61 and 0.64 for

Fig. 7 - Interdependence between recrystallized grain diameter, D_s, and temperature corrected strain rate, Z. Log Z is normalized at 900°C and 1.0 s^{-1}. The slopes were found to be 0.15 and 0.07 for worked and cast respectively.

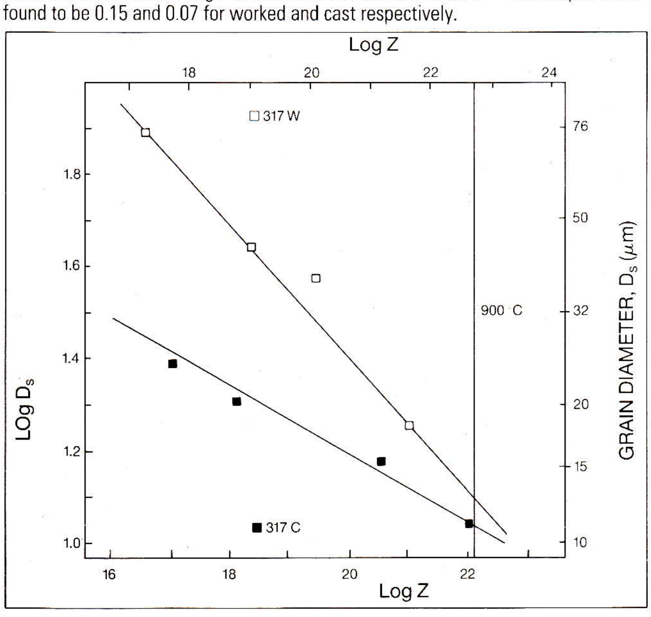

Fig. 8 - Micrographs of substructures:
a) by TEM, 317C: 1) 1100°C, 0.1 s^{-1}; 2) 1100°C, 1.0 s^{-1}; 3) 1100°C 5 s^{-1}; 4) 1000°C, 1.0 s^{-1}.
b) by TEM, 317W, 900°C: 1) 0.1 s^{-1}; 2) 1.0 s^{-1}; 3) 5 s^{-1}.
c) by SEM, electron channeling contrast, 317W: 1200°C, 1.0 s^{-1}.
Elongated subgrains are typical for high Z, and equiaxed subgrains for low Z values. Dynamic recrystallized nuclei and the contribution of particles to static recrystallized grains are evident.

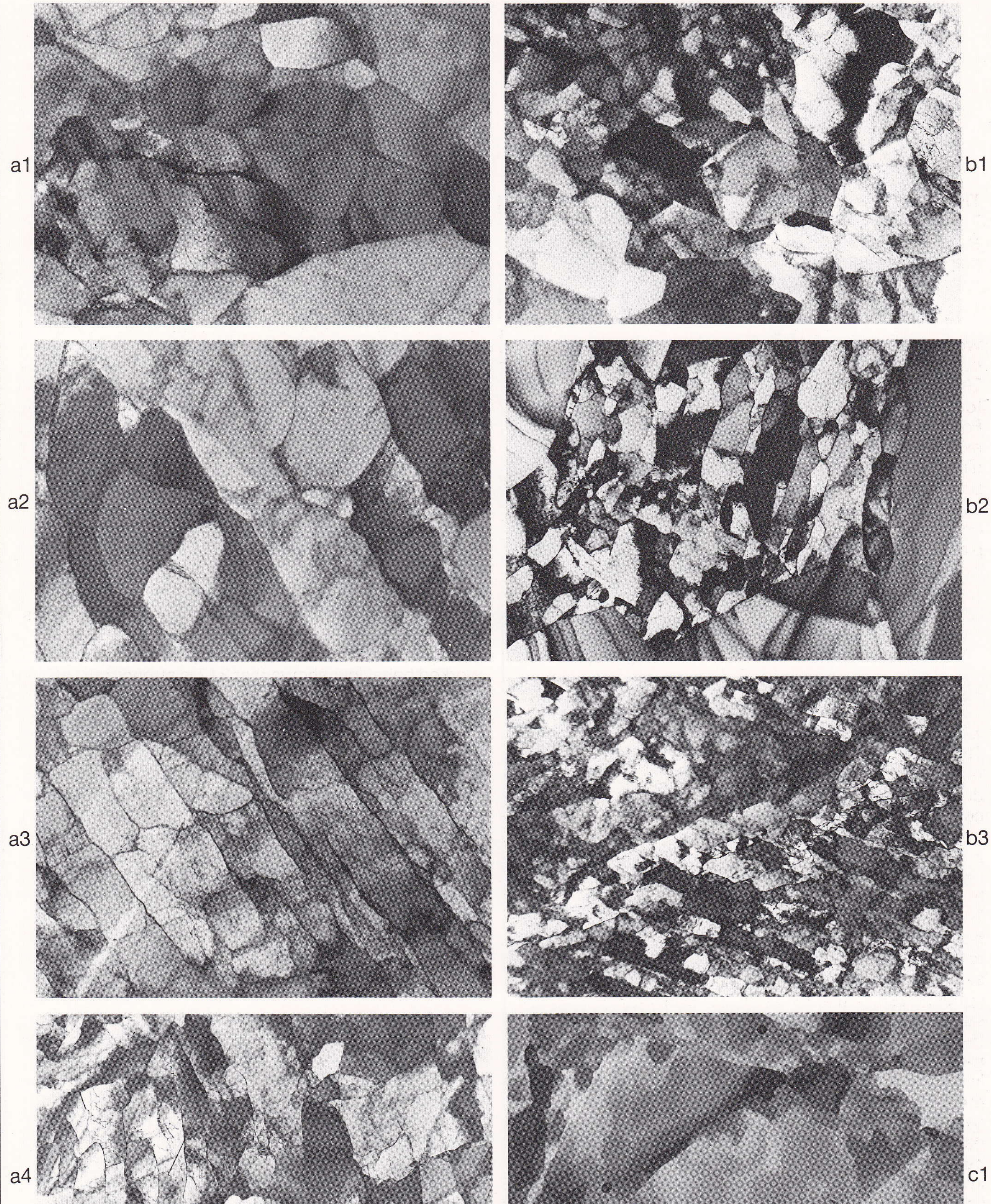

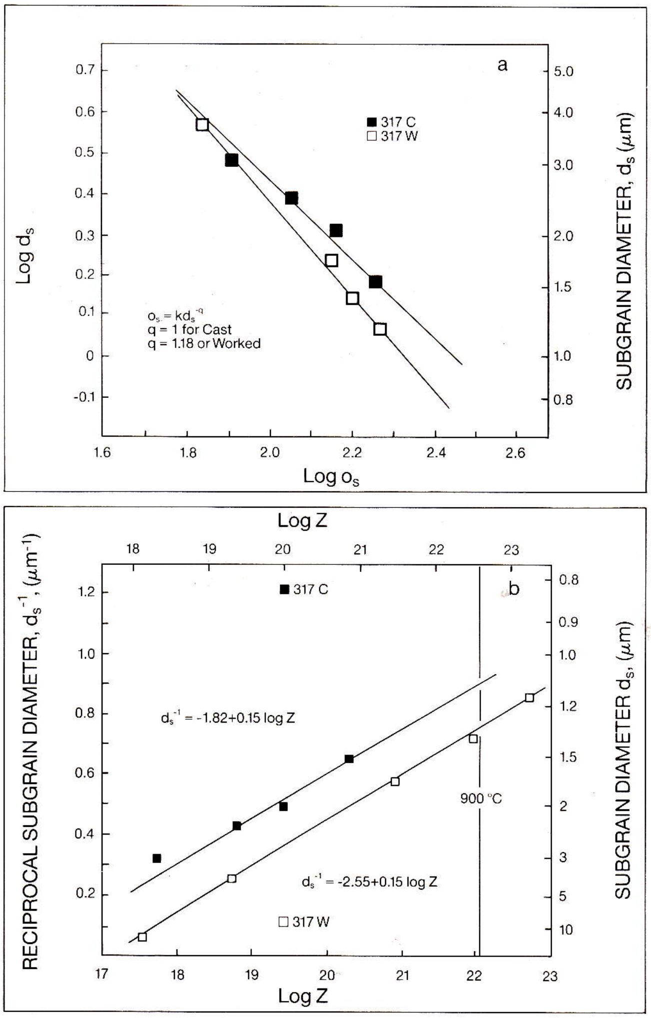

Fig. 9 - Subgrain diameter, d_s, as a function of a) flow stress, b) temperature corrected strain rate, Z. The Z values are normalized at 900°C, 1.0 s^{-1}.

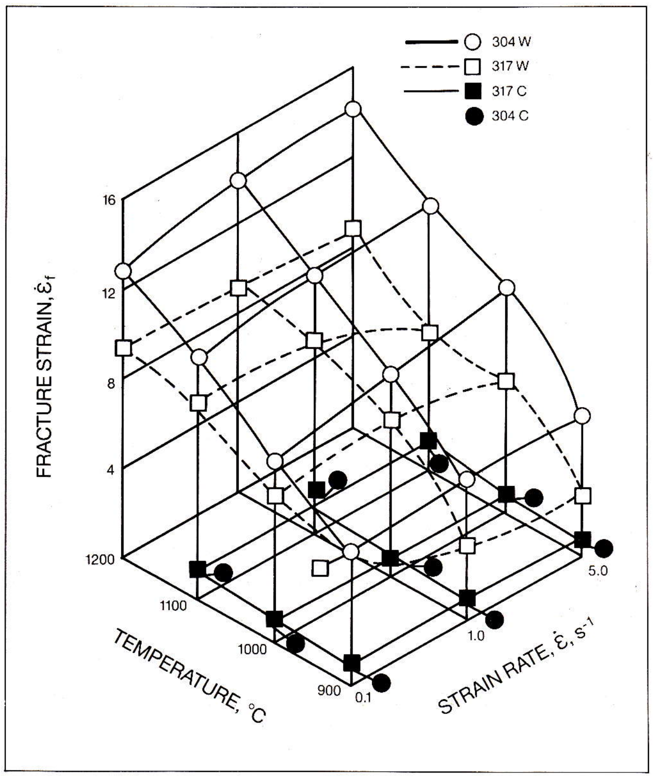

Fig. 10 - Compared to the simpler 304 steel, the ductility of worked 317 is lower. It decreases as temperature declines and strain rate rises because the rate of recrystallization decreases in connection with crack propagation. That of the as-cast material is greatly reduced because δ ferrite and segregates hinder dynamic recrystallization.

304W and 316W respectively. The establishment of σ_s* (Fig. 2) permits one to gauge the maximum softening that DRV could attain under each condition. Comparison of σ_s* and σ_s of the experimental steady-state regime (Fig. 1) shows how much DRX contributes to the softening (9).

The constitutive equation (Eqn. 3) for 317 has also been found suitable for 301, 304 and 316 with different empirical constants (5-9, 20-22). Moreover, the equation has been shown to apply to either σ_p, σ_s or σ_s*. The activation energy for 317 is higher for the as-cast material showing that the δ particles inhibit DRX more at lower temperatures than at high (Figs. 3,4). Similar relationships between as-cast and worked were observed in other austenitic stainless steels. The 317 activation energy of about 500 kJ/mol compares with 400 and 450 kJ/mol for 304 and 316 respectively. The high Q is indicative of a large increase in flow stress as the temperature drops from 1200 to 900°C. Thus the rolling of 317 generates significantly higher forces and torques than 304 or 316 especially in the finishing stages. On the other hand, when slabs are rolled in a planetary mill, the rate of processing generates so much heat that the temperature remains above 1200°C so that the power requirement for 317 is only 18% higher than that for 304, although the activation energy is 25% higher (23). With respect to thermally activated mechanisms, the rise of Q with solute and particle content in the order 304, 316 and 317 indicates how solutes and precipitates slow down the restoration mechanisms (2).

In Fig. 5, the final flow stress, in the steady state for worked 317 and at fracture for the as-cast metal, varies strongly with temperature throughout the entire temperature range studied. This reflects the degree of strain hardening remaining after the effects of DRV and DRX (1,14). The difference between the as-cast and worked values shows the additional hardening due to the larger quantity and elongated shape of δ and the limitation on DRX imposed by its presence. As Z decreases, the as-cast line approaches the worked because of the increased homogenization during working. The yield stress curves exhibit an athermal region at low temperatures, commencing at about 90 MPa for as-cast and at 110 MPa for the worked alloy, reflecting the influence of different fractions of δ phase. At high temperatures, the spacings of σ_y and σ_s curves diminish as restoration reduces the level of strain hardening. In this behaviour, the 317 is similar to the 304 and 316 steels.

The optical micrographs (Fig. 6) reveal the occurrence of DRX and its production of equiaxed grains whose dimensions depend only on the temperature and strain rate.

In the as-cast specimens, the recrystallization is not complete because fracture intervenes. The size is affected by this, because it was not possible to define the as yet unrecrystallized regions. The large fraction of elongated δ particles also inhibited the growth of the DRX grains. The TEM micrographs (Fig. 8) revealed that, under most conditions, the hot worked substructure was retained, confirming that these were DRX grains. However, at high temperatures in the worked specimens, the loss of that substructure in some regions indicated that metadynamic (MRX) or static (SRX) recrystallization had occurred. These are distinguished in that the MRX nuclei have formed dynamically (1,24) whereas the SRX ones have formed after deformation stopped. They both grow after deformation is terminated. However, the MRX ones often cease growing before all the substructure is consumed, because of the presence of some retained substructure within them.

The DRX grain size is almost inversely proportional to the flow stress, as can be seen in Fig. 7. This behaviour of 317 is similar to those of 304, and 301 (9,22); however, its grain size is finer, consistent with the subgrain sizes in Fig. 9b. This relationship has been observed in many other metals and has also been shown to be unaffected by the original grain size (1,17,18). This almost universal relationship of DRX grain size to stress (Eqn. 4) arises from the more fundamental relationship between subgrain size and flow stress (Eqn. 6). In hot working where T and ε are controlled, the value of Z defines the substructure dimensions (Eqn. 5). The latter then determines the flow-stress that develops as the strain progresses both during the strain hardening stage and also during the steady state regime. The subgrains also serve as nuclei for the DRX grains creating the link between D_s and σ_s. The relationship is not based on the Petch effect, since grain boundaries do not offer much constraint to slip transfer at elevated temperatures.

Conclusions

In the hot working of as-cast and worked 317, as for other austenitic stainless steels, the flow stress is reduced by both dynamic recovery and dynamic recrystallization. The 317 alloy is stronger and less ductile than 304 because of higher levels of solute, carbides and δ phase. In the cast material, the δ phase raises the strain hardening yet decreases ε_p; by impeding dynamic recrystallization, which usually retards boundary cracking, it reduces the ductility. The subgrain size is related inversely to the steady-state flow stress and gives rise to a similar relationship between dynamically recrystallized grain size and flow stress. The subgrain and grain sizes are smaller than for type 304 under similar conditions.

Acknowledgements

Support of this work by Consiglio Nazionale delle Ricerche (Italy) and the Natural Sciences and Engineering Reseach Council (Canada) is gratefully acknowledged. The authors are indebted to Comitato Tecnologico (C.N.R.) and Università di Ancona for visiting grants.

REFERENCES

(1) *McQueen, H.J., and J.J. Jonas. Recent advances in hot working: Fundamental dynamic softening mechanisms.* ***J. Appl. Metalwork. 3*** *(1984), 233-241.*

(2) *McQueen, H.J., and J.J. Jonas. Role of dynamic and static softening mechanisms in multistage hot working.* ***J. Appl. Metalwork. 3***, *(1985) 410-420.*

(3) *Ahlblom, B., and R. Sandström. Hot workability of stainless steels: influence of deformation parameters, microstructural components and restoration processes.* ***Int. Met. Rev. 27*** *(1982), 1-27.*

(4) *Roberts, W. Microstructure evolution and flow stress during hot working. In H.J. McQueen et al. (Eds.),* ***Strength of Metals and Alloys.*** *(ICSMA 7). Pergamon Press, Oxford, 1986, vol. 3, pp. 1859-1891.*

(5) *Ryan, N.D., H.J. McQueen, and J.J. Jonas. The deformation behaviour of type 304, 316, 317 austenitic stainless steels during hot torsion.* ***Can. Metal. Quart. 22*** *(1983), 369-378.*

(6) *Ryan, N.D., and H.J. McQueen. Comparative hot working behaviour of 304, 316 and 317 steels as cast and worked. In*

Development in Stainless Steels Technology. ASM, Metals Park, Ohio, 1985, pp. 293-304.

(7) Ryan, N.D., and H.J. McQueen. Effects of alloying upon the hot workability of carbon, microalloyed, tool, and austenitic stainless steels. **J. Mech. Work. Techn. 12** (1986) 279-296.

(8) Ryan, N.D., H.J. McQueen and E. Evangelista. Dynamic recovery and strain hardening in the hot deformation of type 317 stainless steel. **Mat. Sci. Engin., 8** (1986), 259-272.

(9) Ryan, N.D., H.J. McQueen, and E. Evangelista. Dynamic recrystallization in austenitic stainless steel. In N. Hansen et al. (Eds.), **Annealing processes-recovery, recrystallization and grain growth.** Roskilde, 1986, pp. 527-534.

(10) Fulop, S., K.C. Cadien, M.J. Luton, and H.J. McQueen. A servo-controlled hydraulic hot-torsion machine for hot working studies. **J. Test. Eval. 5** (1977), 419-426.

(11) Robbins, J.L., O.L. Shepard, and O.D. Sherby. Torsional ductility and strength of iron carbon alloys at elevated temperatures. **Trans. ASM 60,** (1967), 205-216.

(12) Young, C.M., and O.D. Sherby. Subgrain formation and subgrain strengthening in iron-based materials. **J. Iron Steel Inst. 211** (1973), 640-647.

(13) Evangelista, E., H.J. McQueen, and E. Bonetti. Interaction between $(MnFe)Al_6$ particles and substructure formed during hot working of Al-5Mg-0.8Mn alloy. In J.B. Bilde-Sorensen et al. (Eds.), **Deformation of Multi-phase and Particle Containing Materials.** Roskilde, 1983, pp. 243-270.

(14) Mecking, H., and G. Gottstein. Recovery and recrystallization during deformation. In F. Haessner (Ed.), **Recrystallization of Metallic Materials.** Dr. Riederer Verlag, Stuttgart, 1978, pp. 195-220.

(15) Carfi, G., C. Perdrix, D. Bouleaux, and C. Donadille. Microstructure evolution of AISI 304L grade stainless steel during isothermal straining by hot torsion. In H.J. McQueen et al. (Eds.), **Strength of Metals and Alloys.** (ICSMA 7). Pergamon Press, Oxford, 1986, vol. 2, pp. 929-934.

(16) Wray, P.J. Onset of recrystallization during the tensile deformation of austenitic iron at intermediate strain rates. **Met. Trans. 6A,** (1975), 1197-1203.

(17) Sellars, C.M., and W.J. McG. Tegart. Hot workability. **Int. Met. Rev. 17** (1972), 1-24.

(18) Sakai, T., and J.J. Jonas. Dynamic recrystallization: mechanical and microstructural considerations. **Acta Met., 32** (1984), 189-209.

(19) Fritzmeier, L., M.J. Luton, and H.J. McQueen. Dislocation substructure in dynamic recovery and recrystallization of hot worked austenitic stainless steel. In P. Haasen et al. (Eds.), **Strength of Metals and Alloys.** (ICSMA 5). Pergamon Press, Oxford, 1979, vol. 1, pp. 95-100.

(20) McShane, H.B., and T. Sheppard. On the elevated-temperature constitutive relationship and structure of austenitic stainless steel. **J. Mech. Work. Technol. 9** (1984), 147-180.

(21) Ryan, N.D., and H.J. McQueen. Hot deformation of 301 steel. In H.J. McQueen et al. (Eds), **Strength of Metals and Alloys.** (ICSMA 7). Pergamon Press, Oxford, 1986, vol. 2, pp. 935-940.

(22) Ryan, N.D., and H.J. McQueen. Hot deformation characteristics of worked types 301 and 304 austenitic stainless steels. In S. Blecic et al. (Eds), **Plasticity and Resistance to Deformation.** Univ. of Titograd, 1986, pp. 11-26.

(23) Ryan, N.D., and H.J. McQueen. Calculation of power requirement for hot rolling stainless steels in a planetary mill. Proc. of the **4th Steel Rolling Conference.** France, 1987.

(24) Djaic, R.A.P., and J.J. Jonas. Static recrystallization in austenite between intervals of hot deformation. **J. Iron Steel Inst. 212** (1972), 256-261.